
Article:
Gooding, JD, Crook, R and Tomlin, AS (2015) Modelling of roof geometries from low-resolution LiDAR data for city-scale solar energy applications using a neighbouring buildings method. Applied Energy, 148. pp. 93-104. ISSN: 0306-2619

https://doi.org/10.1016/j.apenergy.2015.03.013

Modelling of Roof Geometries from Low-resolution LiDAR Data for City-Scale Solar Energy Applications using a Neighbouring Buildings Method

James Gooding, Rolf Crook, Alison S. Tomlin*

*Corresponding author, a.s.tomlin@leeds.ac.uk, +44 113 343 2556, Energy Research Institute, School of Chemical and Process Engineering, University of Leeds, LS2 9JT, United Kingdom.

Abstract

This article describes a method to model roof geometries from widely available low-resolution (2 m horizontal) Light Detection and Ranging (LiDAR) datasets for application on a city wide scale. The model provides roof area, orientation, and slope, appropriate for predictions of solar technology performance, being of value to national and regional policy makers in addition to investors and individuals appraising the viability of specific sites. Where present, similar buildings are grouped together based on proximity and building footprint dimensions. LiDAR data from all the buildings in a group is combined to construct a shared high-resolution LiDAR dataset. The best-fit roof shape is then selected from a catalogue of common roof shapes and assigned to all buildings in that group. Method validation was completed by comparing the model output to a ground-based survey of 169 buildings and aerial photographs of 536 buildings, all located in Leeds, UK. The method correctly identifies roof shape in 87% of cases and the modelled roof slope has a mean absolute error of 3.76°. These performance figures are only possible when segmentation, similar building grouping and ridge repositioning algorithms are used.

Highlights

- Automated modelling of roof geometries from low-resolution LiDAR data
- 87% success rate in recognition of roof shape
- Roof slope estimated with 3.76° mean absolute error
- City-scale applicability
- Improves accuracy of solar photovoltaic installation performance predictions

Keywords

Solar; LiDAR; Urban landscape; City; Microgeneration

1 Introduction

Photovoltaics (PV) and solar water heating are two climate change mitigation technologies that can be installed on the rooftops of individual properties and offer substantial emission savings [1, 2]. The sector has experienced tremendous growth in recent years [3-5] but its expansion remains mostly dependent on a very large number of decisions to invest in separate projects [6]. The absence of reliable performance projections has been identified as a major barrier to the uptake of low carbon technologies among individuals [7], landlords and local governments [8]. The roll-out of solar technologies on a city wide scale could be supported by mapping the feasibility of solar installations [7] to influence not only individual property owners but also those responsible for entire portfolios.

This process must be supported by accurate installation performance projections [9, 10] not on a case-by-case basis, but at the city scale where many thousands of potential investment decisions require information.

The city wide approach has further advantages beyond influencing small-scale investment as policy makers would have access to estimations of the regional and national potential of the technologies underpinned by locally accurate appraisals from the city-scale. This could move decision making away from top-down studies based on generalised socio-economic trends that, by their nature, cannot be inspected to the individual property level.

The accurate appraisal of a proposed solar installation's performance requires detailed knowledge of the property's geometry and positioning [11]. Height above sea level LiDAR data aggregated into a digital surface model (DSM) is a data source that can be used to estimate this information for buildings across an entire city as various sources demonstrate [12-15]. Resolution is critically important when attempting to model the slope, orientation and available area of roofs as it controls the amount of height data available for the appraisal of each building. Currently in the UK, the availability of DSMs with a horizontal resolution finer than 2 m is limited to small areas of cities at prohibitively high costs. We previously reported that more widely available low-resolution 2 m data is too coarse to provide an accurate reflection of the number of roof planes and their angles when the plan area of a building is less than approximately 200 m^2 [16]. This is particularly problematic for city-scale roof shape modelling given that building footprint data for Sheffield, a typical UK city, shows that over 70% of properties fall below this threshold [17]. This is a fundamental problem because it is at these properties where the greatest interest in microgeneration investment lies.

DSM data collection processes detect overhanging trees, chimneys and dormer windows which lead to inaccuracy in the assessment of building height and is exacerbated by the incumbent vertical error of the measurements that can be as great as 0.15 m [18]. This is significant as small property roofs are typically less than 3.5 m in height from eave to ridge. In addition, the datasets are also prone to noise and poor geospatial referencing. These issues mean that small property roof shapes and the angles of their facets are inaccurately appraised using low-resolution DSM data and basic interpolation. Due to these problems the most suitable approaches to roof reconstruction from low-resolution DSM data are model-driven methodologies as opposed to data-driven ones. The two types of methodology have been defined by Maas and Vosselman [19]. Data-driven methodologies establish planes directly from the DSM or following a small degree of alteration. By contrast, model-driven approaches compare DSM data to a series of common roof shapes, or 'templates', with the quality of fit quantified, and the best performing template accepted as the modelled roof shape. Tarsha-Kurdi et al. [20] provide analysis and comparison of both approaches to further aid distinction between the two, stating that data-driven methods have a fundamental assumption that buildings are an aggregation of several segmented roof planes. Model-driven methodologies however, test the quality of fit when matching raw data to the most similar roof shape from a library of pre-defined shapes. This means that a model-driven methodology will always return a logical roof shape whereas data-driven methods have been found to misinterpret low-resolution data and suggest a large number of nonsensical roof facets on each property [21].

2 Method

Here we describe a methodology that builds on previous model-driven approaches by incorporating a number of novel elements. We first apply segmentation processes to building footprint data in order to remove peripheral building components, thus disregarding small building protrusions (<20 m^2) that are unsuitable for solar technologies. The resulting segmented building footprints are assumed to define locations within the DSM containing roof-space potentially suitable for solar technologies. They are also used to estimate orientation and to provide a basis for identifying similarities in the roof shapes of neighbouring properties. Buildings within the same 250 m x 250 m areas are then grouped together if their segmented building footprint dimensions are similar. There is then a process to combine the DSM data from properties of the same group, thus creating a pool of DSM data of a finer resolution than from the original individual properties. The combined data is then compared to a series of common roof shapes in a model-driven approach, with the best fit selected as the modelled roof shape in a similar method to that of Huang et al. [22], Lafarge et al. [23] and Henn et al. [24]. Where there are no similar buildings to a particular property, outliers from the segmented individual building's data are removed before the ridge repositioning and template comparison proceed.

The outputs of the methodology are the shape, slope, orientation and plan and sloped area of roofs in a study area. As such, the methodology can also better inform three-dimensional city models which have a wide variety of applications including solar resource estimation. The modelled data are validated against measured data from a large number of buildings within the city of Leeds, UK. The method has been designed for application on a city wide scale meaning it can be implemented for a large number of buildings using only moderate computing power. Furthermore, its use of commonly available low-resolution DSM and building footprint data mean its application may be viable in more locations than those requiring finer resolution data.

2.1 Footprint Segmentation

This process aims to establish the largest rectangle that can be inscribed in the original building footprint. Since the DSM only provides height above sea-level information, the boundaries of each property are established using building footprint data sourced from Digimap [25]. The footprint data is of sufficient detail to include conservatories, porches and other protrusions on small properties which are unlikely to be suitable for solar installations. In addition, such building features can confuse template matching processes as they lead to a wide variety of height measurements across a building which are not representative of the main roof shape.

Segmenting polygons into simple shapes is a basic problem in computational geometry with a body of literature describing potential solutions for specific conditions. A first level of complexity was explored by Fischer and Höffgen [26] who examined inscribing axis-parallel polygons to convex polygons. Daniels et al. [27] and Boland and Urrutia [28] presented methodologies of greater complexity that consider polygons containing both concave and convex angles but still only accept axis-parallel inscribed rectangles which may not define the largest possible rectangle. Conversely, Knauer et al. [29] and Molano et al. [30] have recently explored the problem of computing the largest rectangle of any orientation but only with regard to convex polygons. Hence despite the range of approaches, no single methodology provides a definitive solution to the particular problem faced in this work. However, the building footprint data consists of polygons with characteristics that can be exploited to create a relatively simple and computationally efficient solution. For instance,

the small property polygons never feature internal holes, a large (>16) number of vertices or more curved than straight lines which all increase computational time [30]. There also tends to be a right-angled vertex of the original building footprint that forms part of the largest rectangle that could be inscribed. Utilising these traits, the processes described in the following sections were developed for polygon types of differing complexity.

2.1.1 Polygon Type 1

Polygons with internal angles that are all approximately 90 or 270° are segmented by proposing locations for a fourth vertex of a protrusion in the original building footprint outline. Concave angles in the footprint outline are identified (Figure 1A) as starting points for two intersection lines (Figure 1B), the first of which runs from the vertex preceding the concave angle, through the concave angle itself and on to its intersection with the polygon outline (Figure 1B grey line). The second line proceeds from the vertex following the concave angle through the concave angle and on to its intersection with the polygon outline (Figure 1B black line). The intersection point of the shorter line defines the fourth vertex of a smaller shape within the building footprint (marked with a cross in Figure 1B).

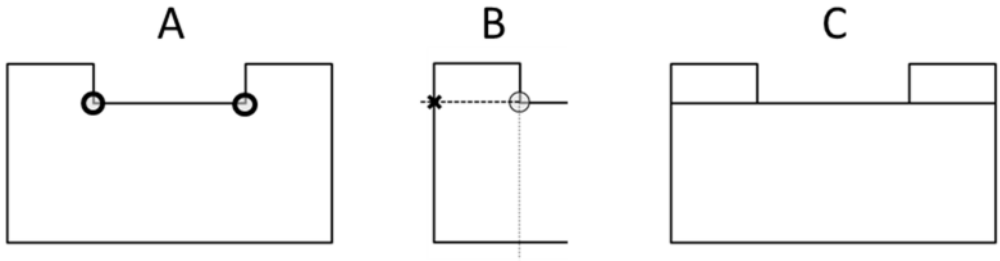

Figure 1 Segmentation process from concave angles. A: Two concave angles circled. B: Creation of intersection lines from a concave angle and identification of an intersection point (denoted by cross) on the shortest. C: Final segmented shape after intersection process repeated for the second concave angle

Figure 1C shows a polygon with two segmented protrusions and a large rectangle that is assumed to define the location of the building's main roof part in the DSM.

2.1.2 Polygon Type 2

The process described above fails on polygons with internal angles that are not 90 or 270° (Figure 2A). For such polygons a second process is presented in which a rectangle is expanded from an internal right-angle of the footprint outline. First, the longest pair of lines to form a right angle in the original building footprint (Figure 2B bold line) are identified and used to project a fourth vertex of a new rectangle (Figure 2C dotted lines) that will be referred to as the 'large rectangle'.

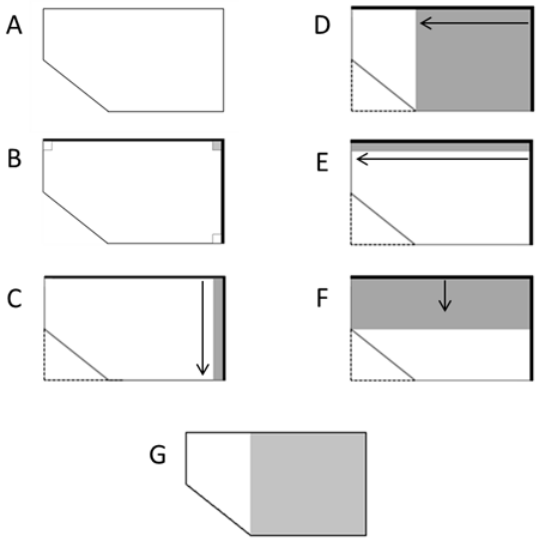

Figure 2 A: Original footprint. B: Longest pair of lines to form a right angle (bold line). C: Large rectangle (dotted lines) formed from the longest right-angled lines. Also shows iterative expansion of a new, inner rectangle along width of large rectangle. D: Second expansion along length of large rectangle. E & F: Repetition of expansion process (length first). G: Larger shape created by the two expansions (in grey) accepted as main roof part of original footprint.

A 0.5 by 0.5 m rectangle is constructed at the intersection of the two longest lines to intersect at a right-angle (Figure 2B, grey square) that will be referred to hereafter as the 'new rectangle'. The new rectangle is expanded in increments of 0.1 m along the width of the large rectangle until it no longer fits inside the original building footprint (Figure 2C). The enlarged new rectangle is then expanded in increments of 0.1 m along the length of the large rectangle again until it no longer fits inside the original building footprint (Figure 2D) which defines a first inscribed rectangle. The double expansion process is then repeated but with extension by length preceding the enlargement in width (Figure 2E & F) to create a second inscribed rectangle. The larger of the two inscribed rectangles is selected as the best approximation for the location of the property's main roof structure from within the original building footprint (Figure 2G, grey rectangle).

2.1.3 Polygon Type 3

A small proportion of polygons fail the criteria of the processes described above, an example of which has been provided in Figure 3.

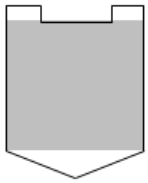

Figure 3 Polygon (black outline) containing interior angles not approximately 90 or 270° and without right-angled vertices in common with the final desired segmented polygon (grey rectangle)

Here the interior angles are not all approximately 90 or 270° and do not share right angles in common with the final segmented polygon. A brute force method is implemented for these polygons whereby a small rectangle is expanded and rotated incrementally from the centre of the original building footprint until it occupies the largest space of the original building footprint. There is no prior information to deduce if a building footprint shares any vertices in common with its final segmented building footprint so if the polygon is not type 1, the processes for polygon types 2 and 3

must both be executed. The larger inscribed polygon resulting from the two processes is accepted as the segmented building footprint.

The solutions for polygon types 2 and 3 are iterative procedures that reflect the lack of an elegant mathematical solution for this problem. The resulting modified building footprints are more suitable for identifying the location of roof shapes suitable for solar technologies within the DSM for extraction. Figure 4 shows an example of the outcome of the segmentation process when applied across a neighbourhood.

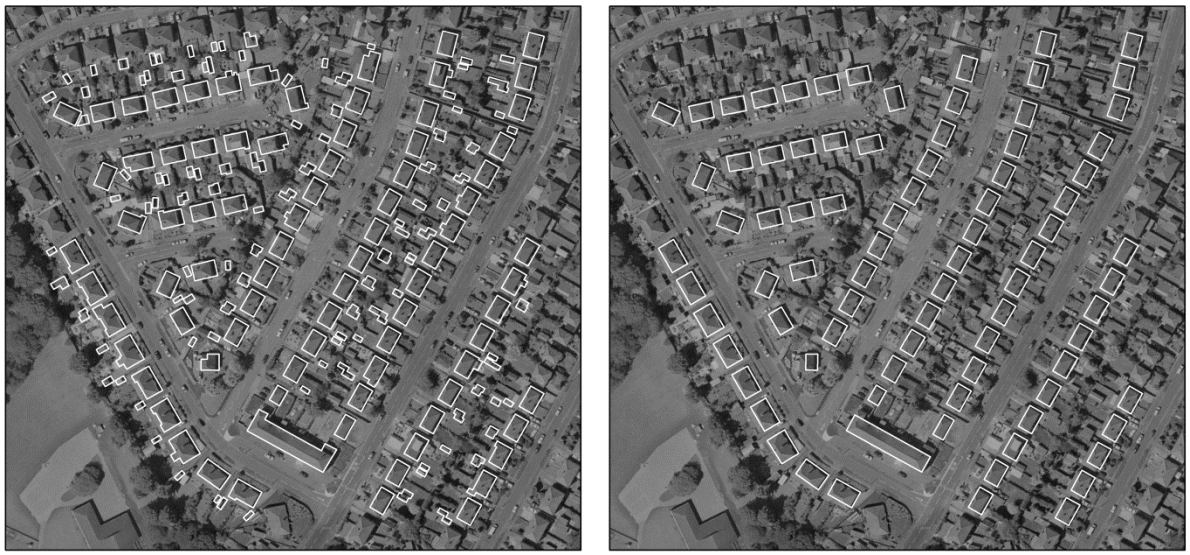

Figure 4 Segmentation of building footprint data (left) across a neighbourhood to extract major roof parts (right) in neighbourhood 690

The segmented polygons also provide a way to assess the size and orientation of roof structures, saving significant computational time compared to Huang et al. [22] who use only DSM data and find building locations by 'blob detection' and size and orientation by localised iteration.

2.2 Data Combination Procedures

It is important to note here that the combination of data is limited to neighbourhoods where there are similar buildings. The DSM data from buildings that do not share a similar neighbour still undergo the processing steps outlined below and are then compared to a series of roof templates without any combination of data and thus remain at low resolution.

2.2.1 Similarity Identification

The dimensions of the segmented building footprints are used to identify similar shapes within 62,500 m^2 neighbourhoods. The buildings are categorised using bins of 1.1 m for length and 1.2 m for width which were empirically found to be robust thresholds to group similar buildings together. Buildings within the same bins for both dimensions are assigned to the same similarity group to have their DSM data combined following further processing.

The following paragraphs describe how the tightly constrained plan dimensional thresholds enable the grouping of buildings with identical roof shape. For example buildings 1, 2 and 3 in Figure 5 are within the same 62,500 m^2 neighbourhood and have plan dimensions that are alike, but building 3 has a different roof type (hipped) to 1 and 2 (both gabled).

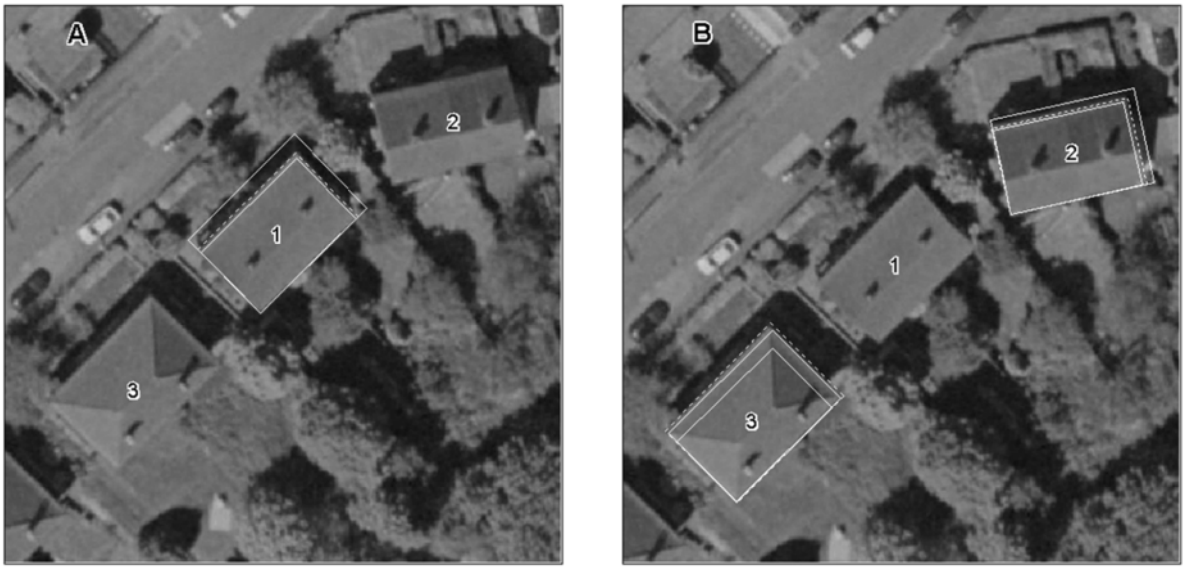

Figure 5 Similarity thresholds. The small, solid white rectangles have the shortest length and width of the bin to which the building footprint (dotted white line) is a member. The larger, solid white-lined rectangle has the longest length and width of this bin.

The bin sizes used to assign similarity grouping are based on increments of 1.1 m for width and 1.2 m for length. For example, building 1 has a length of 13.05 m and width of 8.28 m and falls in to a bin of 12.58 m to 13.78 m for length and a 7.98 m to 9.08 m bin for width. Figure 5A shows two rectangles constructed around the segmented footprint of building 1 (dotted outline). The smaller white outline has the dimensions of a rectangle with the smallest width and length of their respective bins creating a rectangle 12.58 m in length and 7.98 m in width. The larger white rectangle has dimensions equal to the longest edges of each bin, meaning a length of 13.78 m and a width of 9.08 m. For buildings 2 or 3 to be considered similar to building 1 they must have a segmented footprint that fits between the solid white lines.

Figure 5B shows that the footprint of building 2 fits between the solid white lines meaning it would be considered a similar building. The footprint for building 3 extends out of the two solid lines and so would not be grouped as similar to buildings 1 and 2. The method detects small differences in plan dimensions that reflect differences in building construction and roof shape.

2.2.2 Outlier Identification and Height Normalisation

Building footprint and DSM data are often misaligned which can result in ground height data appearing inside a building footprint or conversely, roof data falling outside and being mistakenly disregarded. DSM data also tends to contain many outliers that must be identified and removed. Therefore, data points with an absolute height difference greater than 1.5 m compared to the average of their neighbours were removed.

DSMs provide height above sea-level measurements which means that data from two buildings cannot be directly combined without first normalising the heights such that they are made relative to ground or eave level. Therefore, the lowest height measurement of each property following the removal of outliers is used to define the roof's minimum height. The relative heights of the building's data points are then established by subtracting this minimum height from each DSM data point contained by the relevant segmented building footprint.

2.2.3 Rotation, Ridge Repositioning and Combination

To enable the combination of similar buildings' data, each segmented building footprint and the DSM data it contains are rotated until the lengths of the footprint are made axis-parallel. The processed DSM data of similar buildings from a neighbourhood are then combined and in doing so a dataset of far higher resolution than the original individual buildings is obtained. The following paragraphs explain how this and the outlier identification algorithm are executed using a gable roof shape template as an example because it is the clearest to visualise. The same approach is applied to the hipped, long hipped and pyramidal templates.

The angle between the horizontal and the most southerly line in the building footprint outline is calculated as are the angle and distance of each DSM data point from the most southerly vertex of the building footprint (Figure 6A). This information is used to re-project the DSM data points into position when the building footprint is rotated to make its length axis-parallel (Figure 6B).

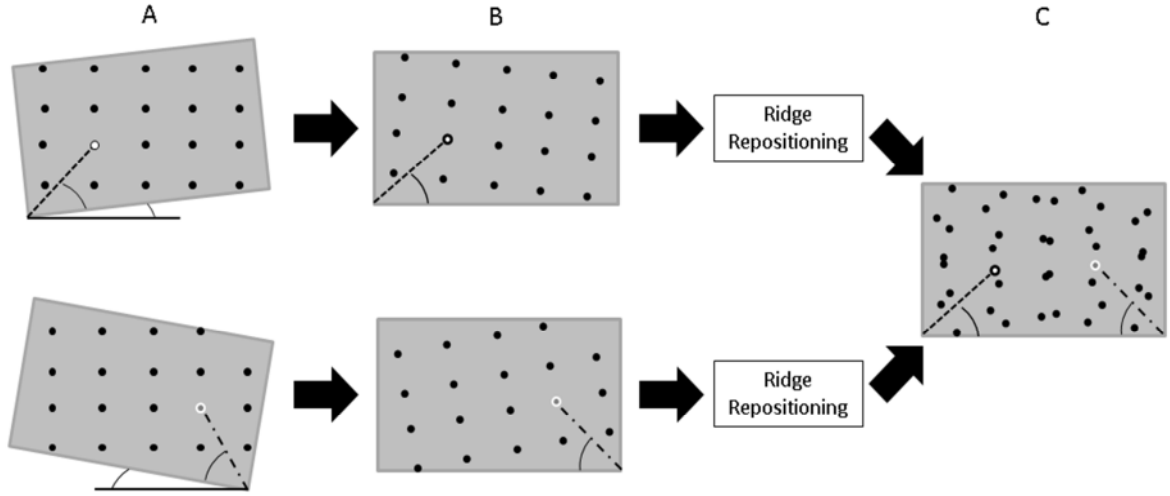

Figure 6 Data rotation and combination procedure

The rotated data is used to assess the true position of roof ridges in the data extracted from the DSM using each building footprint. Due to misalignment between the building footprint data and the DSM, the geometric centre of a segmented building footprint is often not the location of the tallest DSM data as would be expected for a symmetrical roof with accurate positioning. This problem is addressed to ensure that data from similar buildings are overlaid correctly. The data is split into 0.7 m bins along the y-axis of rotated data from individual buildings with ridge location identified by the bin containing the highest average DSM data.

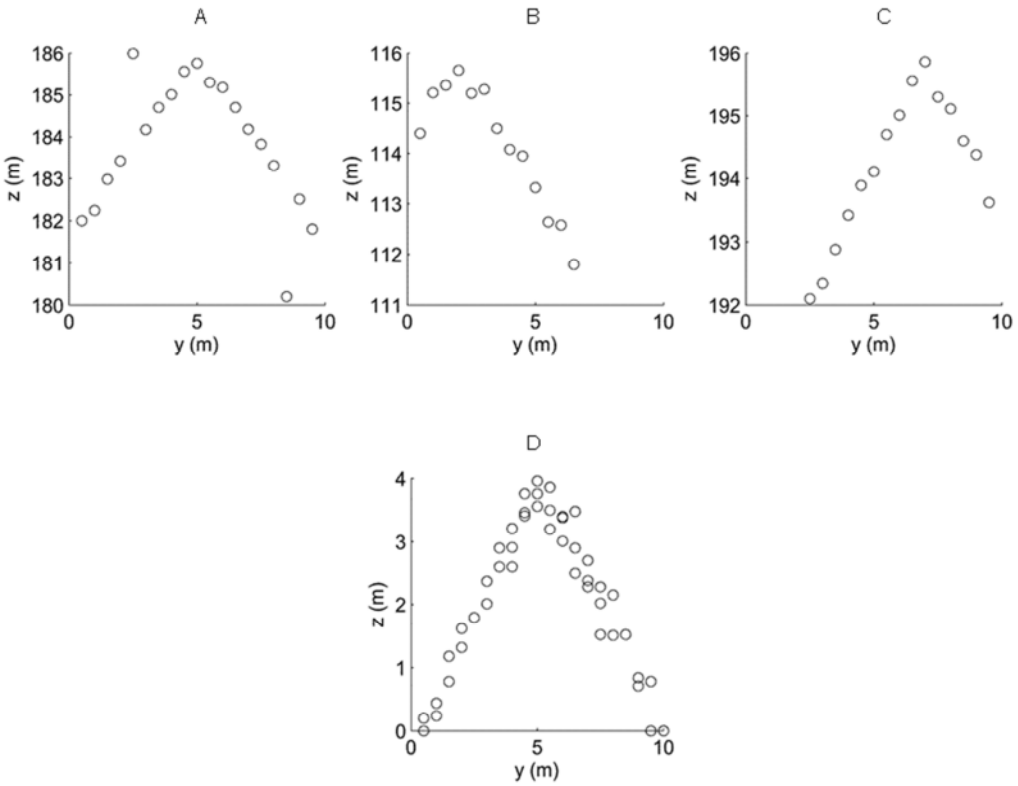

Figure 7 A-C: Rotated DSM data for three similar gable buildings prior to combination viewed from the y, z perspective. D: Combined data following height normalisation, outlier identification and ridge repositioning processes

Figure 7A-C show datasets with issues that must be addressed prior to data combination. Figure 7A has two outlier data points whilst B and C show the outcome of particularly poor alignments between building footprint and DSM data as two aligned datasets would lead to a peak near 5m on the y-axis. Consequently B contains little data for the left hand side of its roof whilst the data in C has no information regarding its lower right hand side. All three datasets must also have their heights normalised prior to combination. The result of the combination procedures is demonstrated in Figure 7D where there is a complete roof profile free of outliers at a far higher resolution than data for individual roofs could provide.

2.3 Template Construction and Selection

The combined data is then compared to the set of common roof shapes shown in Figure 8 with the best fitting selected as the most appropriate model of the similar buildings' roofs.

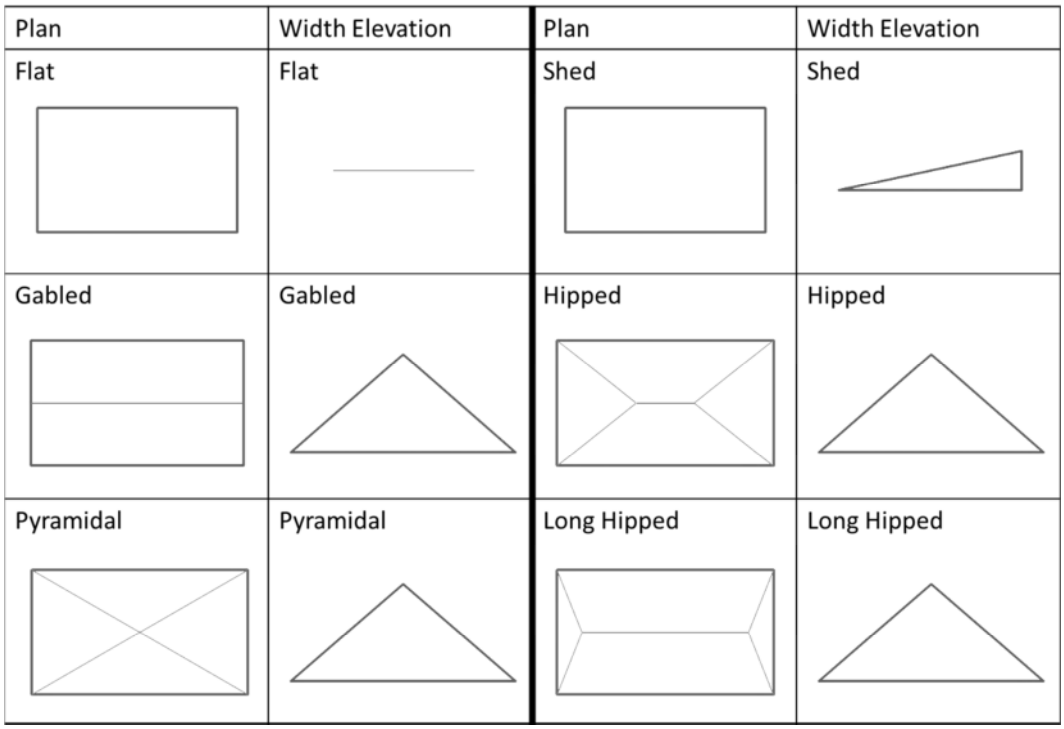

Figure 8 The roof template library

2.3.1 Construction

For a fair comparison the templates are constructed to achieve the best possible fit whilst maintaining the integrity of their shape. Therefore, templates are constructed using the combined data itself to establish eave and ridge heights from which the rest of the model shape is formed.

The data is first divided between the facets of the particular template depending on its x, y position. Facet dimensions are defined by empirical evidence from aerial photography such that, for example, the ridge length is 35% of the footprint length for the hipped template and 68% for the long hipped template. Figure 9 shows a hipped template with four numbered facets.

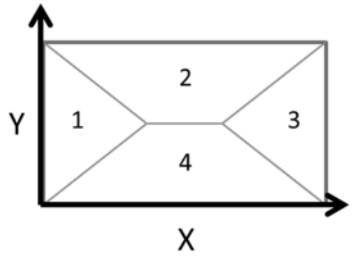

Figure 9 The four regions of a hipped template. 1 and 3: hip sections. 2 and 4: gable sections

Owing to the directions of the template's slopes, the y-axis information is disregarded for sections 1 and 3 of Figure 9 and regression is applied to the x, z data. By contrast, only the y, z data of sections 2 and 4 is analysed. The MATLAB® robustfit function [31] is used to execute an iteratively reweighted least squares fit that reduces the effect of any remaining outliers that were not identified by the outlier identification criterion described in section 2.2.3. However, regression lines alone do not constitute a satisfactorily modelled roof shape because they fail to meet at the same ridge height and do not share a common eave height, which are two essential properties of a logical roof shape. Hence the regression lines are used to establish average eave and ridge heights. Returning to the hipped template example, the lowest and highest points of the four regression lines within the

facets are averaged by weight of the number of data points in their respective facets, thus calculating the average minimum (eave) and maximum (ridge) heights of the prospective template. The eave and ridge heights are then used to define the template's final shape by constructing facets between them appropriate to the template type of plan dimensions relative to the average plan area of all segmented building footprints in the relevant similarity group. At this stage, if the difference in height from eave to ridge is less than 2 m, all templates except flat and shed are rejected.

2.3.2 Selection

The constructed templates are then compared to the combined data using a z-error (Δ_z) metric similar to Huang et al. [22] such that,

$$\Delta_z = \frac{\sum|Z_m - Z_d|}{K} \quad (1)$$

where Z_m is height above eave level suggested by the model, Z_d is the height above eave level of the combined data and K the total number of data points in the combined data. The template with the smallest Δ_z value defines the best fit and provides the modelled angles of facet slopes. The data is compared to each template unless its length is less than 15.9 m, in which case the long hipped template is not tested as in early investigations it was found to bare close similarity to the gable template when scaled for building lengths shorter than this threshold.

3 Validation and Applications

3.1 Data Sources and Test Area

Building footprint data was sourced from EDINA [17], a centre that provides spatial data for UK research institutions [32]. It provides the location and two-dimensional plan view shape of buildings which were used in this study to establish areas of the DSM containing roof height information. The 2 m resolution DSM and aerial photography used in the validation were sourced from Landmap [18], a service that provided UK academia with spatial data until December 2013 [33]. The methodology was applied to seven randomly selected 62,500 m^2 suburban neighbourhood zones in North West Leeds, UK containing a total of 536 buildings. Figure 10 shows four of the neighbourhoods selected.

Figure 10 Four of the neighbourhoods tested using the methodology where the white lines represent the building footprint data prior to segmentation

The accuracy of roof shape and orientation modelling was validated by comparison to aerial photography. Slope estimation accuracy was appraised from site surveys for which a tripod-mounted laser distance measuring device with an accuracy of +/- 20 mm over 150 m was used.

Across the seven tested neighbourhoods, the number of buildings within each grouping ranged from 2 to 68 and averaged 3.9. Typically 35% of buildings had to be regarded as individual for the tested neighbourhoods. It should be noted that this is highly specific to the test locations and that regional variations are to be expected. However, when the segmentation and similarity identification processes were applied to all neighbourhoods across the city of Leeds, a similar figure of 29.2% of buildings were defined as individual.

The similarity grouping criteria proved to be robust as comparison to geo-referenced aerial photography showed only three buildings (0.6%) erroneously grouped with others that did not share the same roof shape despite having similar plan dimensions.

3.2 Model Outputs

An example of the model's outputs is shown for neighbourhood 364 in Figure 11 where the buildings are labelled by their similarity grouping before the modelled shape, angle and areas of each group are described in Table 1. Facet 1 refers to the modelled slope of the gable section of each roof. Where appropriate, facet 2 refers to the angle modelled for a hip roof section.

Figure 11 Neighbourhood 364 labelled by similarity grouping identification numbers

Group	Buildings (no.)	Modelled Shape	Actual Shape	Mean Segmented footprint Plan Area (m^2)	Mean Measured Plan Area (m^2)	Difference (% of Measured Area)	Facet 1 Modelled Slope (°)	Facet 1 Measured Slope (°)	Facet 1 Slope % Error	Facet 2 Modelled Slope (°)	Facet 2 Measured Slope (°)	Facet 2 Slope % Error
1	2	Flat	Flat	40.56	41.54	-2.37	n/a	n/a	n/a	n/a	n/a	n/a
2	1	Flat	Flat	68.98	72.17	-4.42	n/a	n/a	n/a	n/a	n/a	n/a
3	8	Hipped	Hipped	78.60	89.74	-12.42	29.12	29.62	-1.69	26.69	29.82	-10.50
4	1	Flat	Hipped	73.34	87.98	-16.64	n/a	32.5	n/a	n/a	31.29	n/a
5	1	Flat	Flat	46.07	43.59	5.69	n/a	n/a	n/a	n/a	n/a	n/a
6	1	Flat	Flat	199.00	186.5	6.70	n/a	n/a	n/a	n/a	n/a	n/a
7	5	Long Hipped	Long Hipped	158.92	183.78	-13.53	27.76	28.90	-3.94	31.97	29.68	7.72
8	1	Gabled	Long Hipped	152.00	184.09	-17.43	33.49	28.90	-15.88	n/a	29.68	n/a
9	18	Long Hipped	Long Hipped	164.31	184.58	-10.98	28.13	28.90	-2.66	33.45	29.68	12.70
10	2	Long Hipped	Long Hipped	176.50	187.67	-5.95	31.15	30.00	3.83	36.84	32.00	15.13
11	1	Gabled	Gabled	440.30	453.44	-2.90	11.71	11.40	2.72	n/a	n/a	n/a

334 **Table 1 Model output for similarity groups of neighbourhood 364**

For neighbourhood 364, the method successfully modelled roof shape in 39/41 (95.1%) cases. In the two erroneous results, the buildings concerned were regarded as individual buildings and so could only be modelled using the resolution of the input DSM.

The average error in the modelling of plan area for neighbourhood 364 was -6.75% and Table 1 shows that there was a slight underestimation in the majority of cases. This is due to both the inherent inaccuracy of building footprint sizes and the adjustments made to polygons that were not completely rectangular during the segmentation process. Slope was modelled with an average error of 2.36% for facet 1 slopes in neighbourhood 364 whilst facet 2 slopes were modelled with an average error of 6.26%. The greater error in the modelling of facet 2 slopes arises from the reduced amount of data available because of the smaller size of facet 2 compared to facet 1 for the long hipped template.

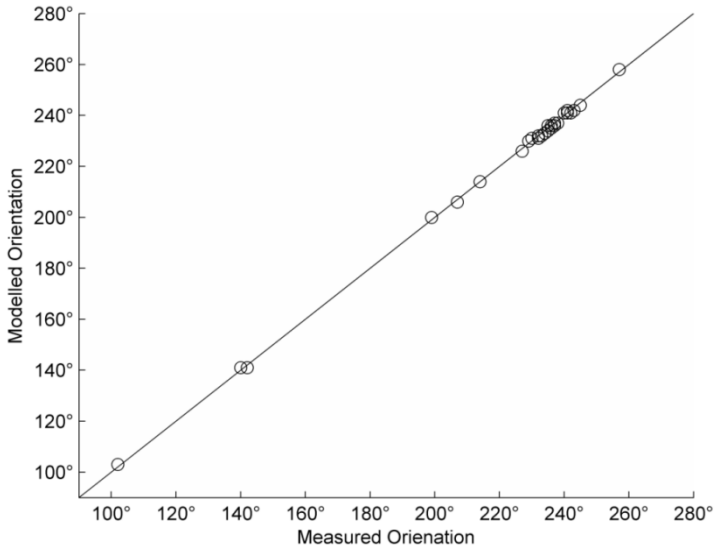

Figure 12 Modelled and observed orientation for neighbourhood 364. Line denotes a 1:1 relationship

Figure 12 shows that for neighbourhood 364, there was an average absolute error of 0.82° (0.39%) in orientation modelling which may result from slight inaccuracies in the positioning of the input building footprint data or slight changes that result from the segmentation process.

3.3 Shape Accuracy

Across all seven tested neighbourhoods, the methodology found the correct shape for 87% of roofs, as shown in Table 2.

Neighbourhood	Total Buildings	Success (No.)	Success (%)
406	83	76	92
759	64	47	73
209	128	110	86
690	84	82	98
867	49	40	80
364	40	38	95
447	88	75	85
Total	536	468	
Average			87

Table 2 Shape matching success in seven tested neighbourhoods

This compares favourably with the one other existing methodology to use low-resolution DSM data by Jacques et al. [21] who achieved a shape matching success rate of 81% based on a study of 242 buildings using a more limited roof template library.

Δ_z was found to decrease when the correct template was compared to data from an increasing number of buildings. Figure 13 provides Δ_z values for five templates as data from an increasing number of hipped roof buildings of a similarity group with eight buildings were combined and compared.

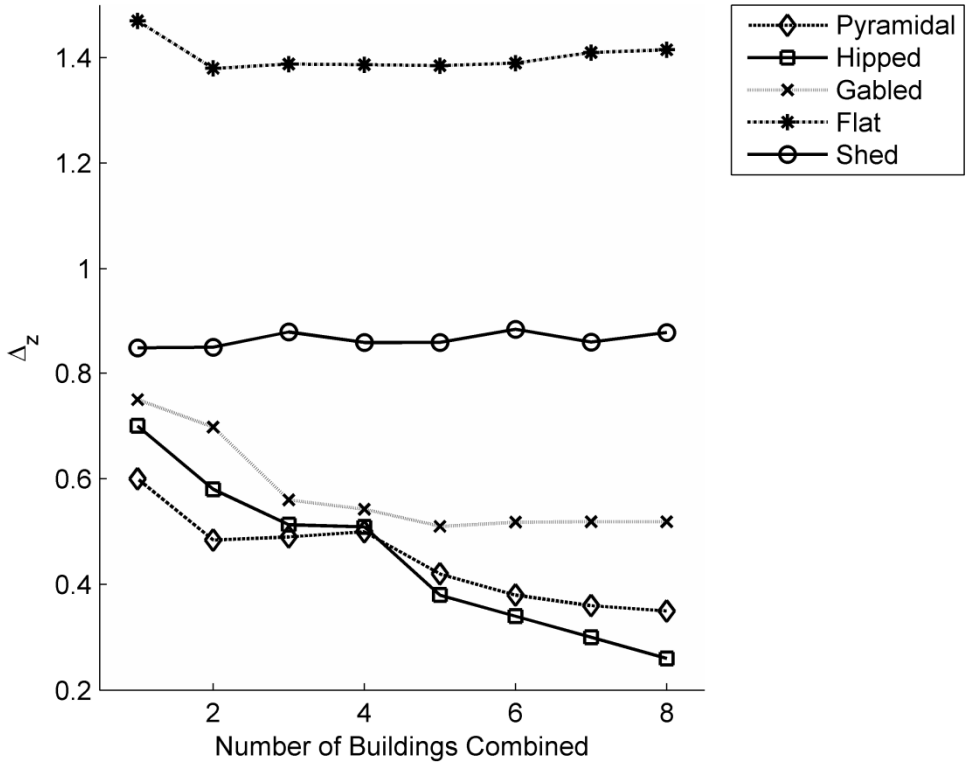

Figure 13 Changes in Δ_z when data from an increasing number of buildings is combined. The correct template is hipped.

The initial trend for pyramidal, hipped and gabled templates is for $\Delta_z$to decrease as data from more buildings are considered in the comparison which signifies an improving fit. It is interesting to note that the correct template (hipped) only scored the lowest Δ_z (and therefore best fit) after the DSM data of more than four buildings were combined. With fewer than five buildings' data, a pyramidal

roof shape would have been incorrectly modelled, demonstrating the key advantage of using multiple similar buildings.

3.4 Slope Accuracy

The facet 1 slopes of the modelled buildings were compared to the angles observed when 169 building roofs were surveyed. The mean absolute error (MAE) of each similarity group between the modelled and surveyed roofs has been calculated using the equation:

$$MAE = \frac{1}{n}\sum_{i=1}^{n}|f_i - y_i| \quad (2)$$

where n represents the number of slope estimations in each neighbourhood, f_i the modelled slope and y_i the observed slope. Table 3 shows that the MAE when averaged across all of the similarity groups in all of the neighbourhoods was 3.76°.

Neighbourhood	Surveyed Angle (°)	Total Buildings	MAE (°)
406	42.0	19	11.07
209	29.5	49	9.50
690	27.6	68	2.29
867	27.5	5	2.22
364	28.9	18	2.66
364	27.5	5	3.94
364	29.62	8	1.69
364	30.10	2	3.83
447	27.04	5	0.09
447	21.65	3	0.26
Total		182	
Average			3.76

Table 3 MAE in slope prediction of 169 buildings from a range of test neighbourhoods

The worst performing group of buildings (neighbourhood 406) had steep roofs of 42°. This could result in an increased probability of outlier identification failure due to the greater difference in height from one data point to the next on a steeper roof. For this reason the outlier identification process may have incorrectly removed data relating to the ridge of the steep roofs leading to a shallower modelled angle than that surveyed.

3.4.1 Comparison to Footprint-Defined Regression

The simplest method to estimate roof slope would be to fit a regression line to the data points provided by each facet of a single building using, for example, the MATLAB® [31] robustfit tool. The expected geometry of the roof would be defined purely from the building footprint such that, for example, the ridge of a gable roof would occur exactly halfway along the width of the building. In this section we compare the slopes predicted for similar individual gabled facets under this more basic method ($\hat{\beta}_{\mathrm{g-RB}}$, where g refers to gable facets and RB signifies the use of robustfit) and the angle modelled when the multiple buildings methodology described in the present paper was applied ($\hat{\beta}_{\mathrm{g-MB}}$, where MB denotes the use of multiple buildings). A further comparison is made by applying $\hat{\beta}_{\mathrm{g-RB}}$ to the combined data of the buildings to assess the importance of the features in $\hat{\beta}_{\mathrm{g-MB}}$ other than the combination of DSM data from similar buildings, such as the ridge

repositioning process. The buildings below were from a randomly selected similarity group of gable-roofed buildings and had a slope (β_{g}) of 37° when surveyed, 3.06° greater than $\hat{\beta}_{\mathrm{g-MB}}$.

Building ID	$\hat{\beta}_{\mathrm{g-RB}}$ (°)	$\lvert\hat{\beta}_{\mathrm{g-RB}} - \beta_{\mathrm{g}}\rvert$ (°)
2	25.51	11.49
34	8.44	28.56
41	29.07	7.93
44	33.44	3.56
48	35.40	1.60
49	31.03	5.97
Average	27.15	9.85
$\hat{\beta}_{\mathrm{g-RB}}$ Combined	28.50	8.50

	$\hat{\beta}_{\mathrm{g-MB}}$ (°)	$\lvert\hat{\beta}_{\mathrm{g-MB}} - \beta_{\mathrm{g}}\rvert$ (°)
$\hat{\beta}_{\mathrm{g-MB}}$ Combined	33.94	3.06

Table 4 Comparison of modelling gabled roof slopes using building footprint defined MATLAB® robustfit regression on individual and combined data (top) against $\hat{\boldsymbol{\beta}}_{\mathbf{g-MB}}$ (bottom)

From table 4, the average $\lvert\hat{\beta}_{\mathrm{g-RB}} - \beta_{\mathrm{g}}\rvert$ value for individual buildings was 9.85° which is greater than the value for using combined data (8.5°) and substantially larger than the 3.06° value for $\lvert\hat{\beta}_{\mathrm{g-MB}} - \beta_{\mathrm{g}}\rvert$. This shows that the application of the robustfit MATLAB® tool in evaluating geometry derived from building footprints is a less accurate than the methodology presented here, even when the buildings are combined. Whilst a possible cause of the disparity between the two methods is the approach to identifying outliers, the main reason for the improved performance of $\hat{\beta}_{\mathrm{g-MB}}$ is the correction to the misalignment of the two datasets. $\hat{\beta}_{\mathrm{g-MB}}$ compensates for this misalignment by repositioning individual building DSM data prior to combination, enabling a fairer calculation of template suitability.

3.4.2 Benefits of Considering Multiple Buildings When Modelling Slope

Table 5 shows the modelled angles for the gabled ($\hat{\beta}_{\mathrm{g-IND}}$) and hipped ($\hat{\beta}_{\mathrm{h-IND}}$) facets from a randomly selected group of similar buildings with long hipped roof shapes when processed through the methodology individually (IND denotes the use of individual buildings). This means the segmented buildings' DSM data were each passed through the ridge centring, height normalisation and outlier removal processes, but not the rotation and combination procedures. When surveyed, the buildings were found to have gable (β_{g}) and hip (β_{h}) section facets of 27.5°. The final row shows the angles modelled when the data for the five similar buildings was combined and the complete methodology presented here **($\hat{\beta}_{\mathrm{g-MB}}$)** was applied.

Building ID	$\hat{\beta}_{\mathrm{g}}$ (°)	$\left\lvert\hat{\beta}_{\mathrm{g-IND}} - \beta_{\mathrm{g}}\right\rvert$ (°)	$\hat{\beta}_{\mathrm{h}}$ (°)	$\left\lvert\hat{\beta}_{\mathrm{h-IND}} - \beta_{\mathrm{h}}\right\rvert$ (°)
6	22.63	4.87	*	*
13	29.5	2.00	21.99	5.51
18	32.24	4.74	42.07	14.57
19	34.85	7.35	41.27	13.77
28	15.46	12.04	*	*
Average	N/A	6.20	N/A	11.28

	$\hat{\beta}_{\mathrm{g}}$ (°)	$\left\lvert\hat{\beta}_{\mathrm{g-MB}} - \beta_{\mathrm{g}}\right\rvert$ (°)	$\hat{\beta}_{\mathrm{h}}$ (°)	$\left\lvert\hat{\beta}_{\mathrm{h-MB}} - \beta_{\mathrm{h}}\right\rvert$ (°)
$\hat{\beta}_{\mathrm{g-MB}}$	29.72	2.22	33.53	6.03

Table 5 Comparison of slope modelling when buildings were considered individually and when combined. * denotes instances where building shape was incorrectly modelled and did not return an angle for the hipped section of the long-hipped roof template

The average $\left\lvert\hat{\beta}_{\mathrm{g}} - \beta_{\mathrm{g}}\right\rvert$ error in slope estimation is 6.2° which is significantly greater than the 2.22° achieved using $\hat{\beta}_{\mathrm{g-MB}}$. Buildings 6 and 28 of Table 5 are instances in which roof shape was incorrectly modelled as gabled when treated as individual buildings, meaning that no $\hat{\beta}_{\mathrm{h-IND}}$ value was returned, re-illustrating the benefit of using multiple buildings to model shape. Due to their size, the hip sections contain less data than gabled so it is unsurprising that the error in slope estimation is greatest for these parts.

As with roof shape modelling, considering an increasing number of buildings' data for the appraisal of roof slope led to more accurate results. In the following example, the roof slope angle predicted by the model was compared to the angles surveyed on 35 buildings from a range of neighbourhoods with a variety of roof shapes. The key result illustrated by Figure 14 is the general pattern of decreasing errors in modelled slope as data from an increasing number of buildings are combined.

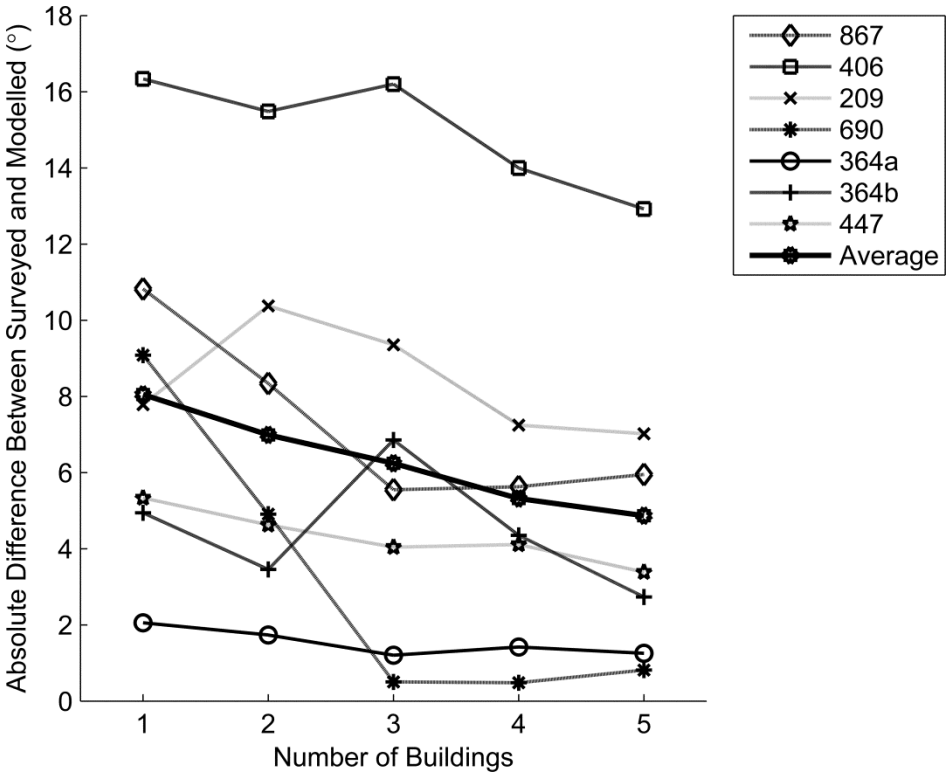

Figure 14 Slope accuracy improvement when using combined DSM data from increasing numbers of buildings. Legend items refer to neighbourhood IDs.

The largest error shown in Figure 14 relates to data from neighbourhood 406 which was characterized by steeper angled roofs. Although requiring further investigation on a larger sample of steep roofs, the results suggest that the method is less accurate on roofs with a slope greater than 40°. Data from such properties have a greater difference in height between neighbouring points and the effect of alterations to the outlier identification criterion should be investigated in future work.

3.5 Suitability to City-Scale Application and Implications for Installation Performance Projections

Using only moderate computing resources, an Intel® Xeon® 3.1GHz processor and 4GB of RAM, the method executed in under three and a half minutes on each neighbourhood including one particularly dense area containing 128 buildings. This suggests it would be suitable for the estimation of potential PV capacity on a city scale. It would however be important to take account of errors in modelled shape and slope in such estimations and this section discusses the potential impact of such errors on the projection of PV installation performance. It is acknowledged that there will be many other factors that influence the performance of solar technologies including shading from surrounding objects and terrain that are beyond the scope of this article which is focused on increasing the accuracy with which area, orientation and slope of roof-spaces are determined from low resolution data.

3.5.1 Slope Errors and Performance Projections

On average over the test areas, the methodology modelled buildings to within 5° of the surveyed slope. Figure 15 shows annual electricity predicted by the EU-JRC PVGIS webtool [34] for a 2.2 kWp system with optimized azimuth for increasing slope, demonstrating a non-linear relationship between the two.

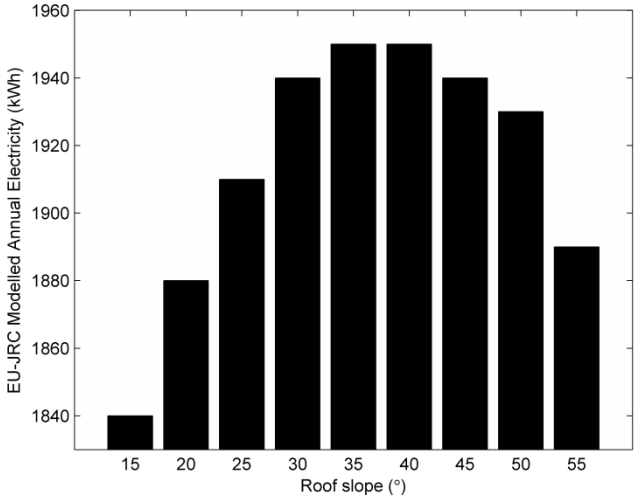

Figure 15 EU JRC PVGIS estimated annual PV power output for a 2.2kWp installation with optimized azimuth under a range of slope conditions

Table 6 shows the range of power output predictions at a range of slope angles for a slope error of ±5° and ±10°.

Roof Slope (°)	% change in predicted annual power output for slope error of ±5° (%)	% change in predicted annual power output for slope error of ±10° (%)
25	3.14	4.71
30	2.06	3.61
35	0.51	2.05
40	0.51	1.03
45	1.03	3.09

Table 6 Difference in EU JRC annual PV power output estimations with changing slope

This shows how sensitive annual power predictions are to errors in slope and in particular, how the sensitivity is greater for the extremes of slope compared to slopes close to the optimum value (approximately 39° for Leeds, UK). As discussed above, the MAE for the tested neighbourhoods using the current method is less than 5° and hence is sufficiently accurate to provide predictions of annual power output even for shallow roof slopes.

3.5.2 Shape Errors and Performance Projections

Available roof area is a function of modelled roof shape and orientation as PV panels are deployed on the most southerly facing roof facets of buildings. This emphasizes the importance of modelling the correct shape of roofs to estimate the performance of PV installations. Figure 16 takes a hypothetical building with a plan area typical of suburban properties (78 m^2) and roof slope of 37.5 ° and investigates the impact on available area if it were modelled as gabled, hipped or pyramidal. The figure is a scaled drawing in which the solar panels are 1 m by 1.6 m and rated at 0.25 kWp to reflect a common PV panel on the market. The darker grey regions on the periphery of the south facing slope represent the area that would be lost if the building were modelled as hipped instead of gabled. The lighter grey regions are the additional south facing area that would be lost if the building was modelled as pyramidal instead of hipped. The inset text states the south facing roof area under each of the templates.

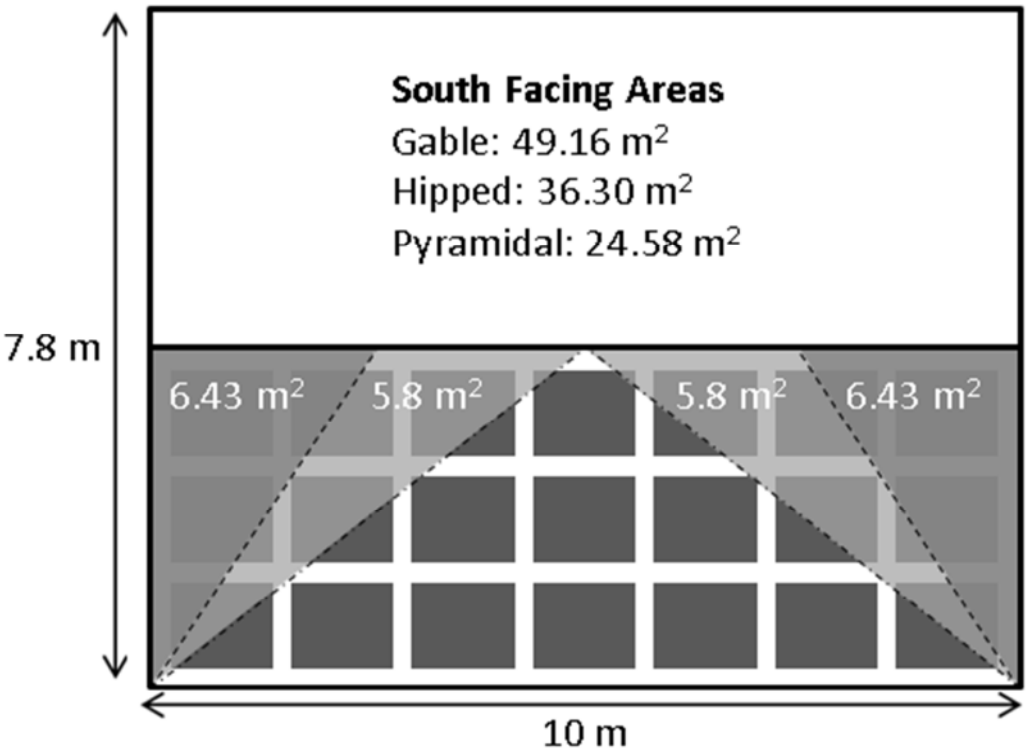

Figure 16 Effect of modelled roof shape on area available for solar technologies

From the available area calculations of Figure 16, the impact of roof shape on annual power output predictions could be investigated. The predicted power outputs shown in Table 7 were again taken from the EU JRC PVGIS tool [34] for a south-facing, 37.5° sloped crystalline silicon panel type without any shading objects in the vicinity.

Modelled shape	Available area (m^2)	System size (kWp)	Predicted Output (kWh a^{-1})
Gable	49.16	5.25	4,560
Hipped	36.30	3.25	2,820
Pyramidal	24.58	2.25	1,950

Table 7 Effect of roof shape modelling on annual power output predictions

Table 7 shows the importance of finding the correct roof shape as it defines the south-facing area available for a PV installation and therefore system size. Power output is clearly far more sensitive to system size than to slope. In the example provided, the reduction in predicted annual power output from a gabled to a hipped property is 37.35%. The reduction if a hipped property were to be modelled as pyramidal is 50.23%, whilst if a property was gabled but incorrectly modelled as pyramidal, there would be a 68.82% loss in predicted output. Hence, achieving 87% success in shape recognition and 3.76° error in slope estimation has been shown to be especially important when seeking to model the potential for PV at every property in a city or for estimating a maximum yield from PV technologies across an entire region.

4 Conclusions

A methodology is presented to model roof shapes using building footprint and low-resolution DSM data. With moderate computing resources the method executes rapidly and so demonstrates high suitability for application across a whole city region.

In 87% of cases tested, the method identified the correct shape of the main roof part of buildings. This was validated using a total of 536 small buildings from different areas of the city of Leeds, UK. The MAE in roof slope was found to be ±3.76° when validated against 182 buildings. Both roof shape and slope were more accurately appraised as greater numbers of similar buildings were incorporated into the combined data set.

Roof slope was defined with greater accuracy than by the application of regression techniques to areas of roofs defined by building footprint data alone. In the example provided, the error of roof slope calculation from the current method was 3.06° whereas using regression on areas of the DSM identified by building footprints led to an average error of 9.85°.

The importance of increased accuracy in modelling roof slope and shape has been discussed in terms of predicted annual PV installation power output with the caveat that there are additional local factors, such as shading, that may affect the performance of solar installations beyond the factors modelled in this methodology. The discussion shows that outputs from the method could be used to calculate payback periods for PV installations on typical residential properties with greater accuracy than previous methodologies.

5 Acknowledgements

This work was financially supported by the Engineering and Physical Sciences Research Council through the University of Leeds Doctoral Training Centre in Low Carbon Technologies. We would also like to thank EDINA and Landmap for the provision of data.

6 References

[1] Bush R, Jacques DA, Scott K, Barrett J. The carbon payback of micro-generation: An integrated hybrid input–output approach. Applied Energy. 2014;119:85-98.
[2] Goe M, Gaustad G. Strengthening the case for recycling photovoltaics: An energy payback analysis. Applied Energy. 2014;120:41-8.
[3] Cherrington R, Goodship V, Longfield A, Kirwan K. The feed-in tariff in the UK: A case study focus on domestic photovoltaic systems. Renewable Energy. 2013;50:421-6.
[4] Muhammad-Sukki F, Ramirez-Iniguez R, Munir AB, Mohd Yasin SH, Abu-Bakar SH, McMeekin SG, et al. Revised feed-in tariff for solar photovoltaic in the United Kingdom: A cloudy future ahead? Energy Policy. 2013;52:832-8.
[5] Chen HH, Lee AHI, Chen S. Strategic policy to select suitable intermediaries for innovation to promote PV solar energy industry in China. Applied Energy. 2014;115:429-37.
[6] Sauter R, Watson J. Strategies for the deployment of micro-generation: Implications for social acceptance. Energy Policy. 2007;35:2770-9.
[7] Bergman N, Eyre N. What role for microgeneration in a shift to a low carbon domestic energy sector in the UK? Energy Efficiency. 2011;4:335-53.
[8] Gouldson A, Kerr, N., Topi, C., Dawkins, E., . The Economics of Low Carbon Cities: A Mini-Stern Review for the Leeds City Region. 2011.

[9] Bull J. Loads of green washing-can behavioural economics increase willingness-to-pay for efficient washing machines in the UK? Energy Policy. 2012;50:242-52.
[10] Kanters J, Wall M, Kjellsson E. The Solar Map as a Knowledge Base for Solar Energy Use. Energy Procedia. 2014;48:1597-606.
[11] Hong T, Koo C, Park J, Park HS. A GIS (geographic information system)-based optimization model for estimating the electricity generation of the rooftop PV (photovoltaic) system. Energy. 2014;65:190-9.
[12] Lukac N, Zlaus D, Seme S, Zalik B, Stumberger G. Rating of roofs' surfaces regarding their solar potential and suitability for PV systems, based on LiDAR data. Applied Energy. 2013;102:803-12.
[13] Jakubiec JA, Reinhart CF. A method for predicting city-wide electricity gains from photovoltaic panels based on LiDAR and GIS data combined with hourly Daysim simulations. Solar Energy. 2013;93:127-43.
[14] Brito MC, Gomes N, Santos T, Tenedório JA. Photovoltaic potential in a Lisbon suburb using LiDAR data. Solar Energy. 2012;86:283-8.
[15] Kucuksari S, Khaleghi AM, Hamidi M, Zhang Y, Szidarovszky F, Bayraksan G, et al. An Integrated GIS, optimization and simulation framework for optimal PV size and location in campus area environments. Applied Energy. 2014;113:1601-13.
[16] Gooding J, Edwards H, Giesekam J, Crook R. Solar City Indicator: A methodology to predict city level PV installed capacity by combining physical capacity and socio-economic factors. Solar Energy. 2013;95:325-35.
[17] [Shape Geospatial Data]. Ordnance Survey (GB); 2011.
[18] Cities Revealed. (c) The GeoInformation Group; 2008.
[19] Maas HG, Vosselman G. Two algorithms for extracting building models from raw laser altimetry data. Isprs Journal of Photogrammetry and Remote Sensing. 1999;54:153-63.
[20] Tarsha-Kurdi F, Landes T, Grussenmeyer P, Koehl M. Model-driven and data-driven approaches using LIDAR data: Analysis and comparison. Munich2007. p. 87-92.
[21] Jacques DA, Gooding J, Giesekam JJ, Tomlin AS, Crook R. Methodology for the assessment of PV capacity over a city region using low-resolution LiDAR data and application to the City of Leeds (UK). Applied Energy. 2014;124:28-34.
[22] Huang H, Brenner C, Sester M. A generative statistical approach to automatic 3D building roof reconstruction from laser scanning data. Isprs Journal of Photogrammetry and Remote Sensing. 2013;79:29-43.
[23] Lafarge F, Descombes X, Zerubia J, Pierrot-Deseilligny M. Structural Approach for Building Reconstruction from a Single DSM. Pattern Analysis and Machine Intelligence, IEEE Transactions on. 2010;32:135-47.
[24] Henn A, Gröger G, Stroh V, Plümer L. Model driven reconstruction of roofs from sparse LIDAR point clouds. Isprs Journal of Photogrammetry and Remote Sensing. 2013;76:17-29.
[25] MasterMap O. Topography Layer [GML geospatial data], Coverage: West Yorkshire. EDINA Digimap Ordnance Survey Service. 2008.
[26] Fischer P, Höffgen K-U. Computing a maximum axis-aligned rectangle in a convex polygon. Information Processing Letters. 1994;51:189-93.
[27] Daniels K, Milenkovic V, Roth D. Finding the largest area axis-parallel rectangle in a polygon. Computational Geometry. 1997;7:125-48.
[28] Boland RP, Urrutia J. Finding the Largest Axis-Aligned Rectangle in a Polygon in. In Proc 13th Canad Conf Comput Geom: Citeseer; 2001.
[29] Knauer C, Schlipf L, Schmidt JM, Tiwary HR. Largest inscribed rectangles in convex polygons. Journal of Discrete Algorithms. 2012;13:78-85.
[30] Molano R, Rodríguez PG, Caro A, Durán ML. Finding the largest area rectangle of arbitrary orientation in a closed contour. Applied Mathematics and Computation. 2012;218:9866-74.
[31] MATLAB. version 7.14.0.739 (R2012a): The MathWorks, Inc.; 2012.
[32] EDINA. Privacy and Cookies Policy. 2013.

589 [33] Landmap. Landmap - Spatial Discovery. 2014.
590 [34] EU-JRC. PV Estimation Utility, European Union Joint Research Council. 2012.

591

592